Nanoporous Silicon Combustion: Observation of Shock Wave and Flame Synthesis of Nanoparticle Silica

Collin R. Becker,*,[†] Greg J. Gillen,[‡] Matthew E. Staymates,[‡] and Conrad R. Stoldt[§]

[†]U.S. Army Research Laboratory, Sensors and Electron Devices Directorate, 2800 Powder Mill Road, Adelphi, Maryland 20783, United States

[‡]National Institute of Standards and Technology, Mail Stop 8371, Gaithersburg, Maryland 20899, United States

[§]Mechanical Engineering Department, University of Colorado, 1111 Engineering Drive, Boulder, Colorado 80309, United States

S Supporting Information

ABSTRACT: The persistent hydrogen termination present in nanoporous silicon (nPS) is unique compared to other forms of nanoscale silicon (Si) which typically readily form a silicon dioxide passivation layer. The hydrogen terminated surface combined with the extremely high surface area of nPS yields a material capable of powerful exothermic reactions when combined with strong oxidizers. Here, a galvanic etching mechanism is used to produce nPS both in bulk Si wafers as well as in patterned regions of Si wafers with microfabricated ignition wires. An explosive composite is generated by filling the pores with sodium perchlorate ($NaClO_4$). Using high-speed video including Schlieren photography, a shock wave is observed to propagate through air at 1127 ± 116 m/s. Additionally, a fireball is observed above the region of nPS combustion which persists for nearly 3× as long when reacted in air compared to N_2, indicating that highly reactive species are generated that can further combust with excess oxygen. Finally, reaction products from either nPS–$NaClO_4$ composites or nPS alone combusted with only high pressure O_2 (400 psig) gas as an oxidizer are captured in a calorimeter bomb. The products in both cases are similar and verified by transmission electron microscopy (TEM) to include nano- to micrometer scale SiO_x particles. This work highlights the complex oxidation mechanism of nPS composites and demonstrates the ability to use a solid state reaction to create a secondary gas phase combustion.

KEYWORDS: porous silicon, ball lightning, nanothermite, nanoenergetic, Raman spectroscopy, MEMS
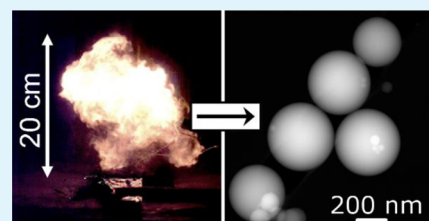
1. INTRODUCTION

The discovery that nanoporous silicon (nPS) is a photo-luminescent material has led to an extremely large and diverse body of research on the material.[1−3] Excitement continues as nPS shows promise for hydrogen storage, fuel cells, solar cells, lithium-ion batteries, sensors, and drug delivery.[4−9] The structure of nPS is readily tunable and is typically formed by electrochemically etching a single crystal silicon (Si) wafer in an electrolyte containing hydrofluoric acid (HF).[1,10] Pore sizes, porosity, and thickness are controlled by the dopant type and concentration of the wafer; the electrolyte concentration and composition; and magnitude of electric current used during etching.[1,10] Additionally, nPS particles can be generated by scraping nPS films from the wafer substrate and placing in an ultrasonic bath to break up the film or by etching metallurgical grade silicon in a bath of nitric acid (HNO_3) and HF.[11,12] With many production options available and possessing unique properties arising from the nanoscale Si domains, nPS can be fine-tuned to serve roles in numerous applications.

The oxidation of nPS is among the most heavily studied aspects of Si oxidation.[13,14] The large surface area of nPS renders the material susceptible to oxidation, which alters the optical, electronic, and chemical properties of the overall material.[15] Of particular interest is the discovery of an explosive reaction of nPS with strong oxidizers including HNO_3 and more recently liquid oxygen.[16,17] Subsequent research has demonstrated similar reactions by filling the pores with solid oxidizers including sulfur and various salts.[18−22] The solid state oxidation reaction makes the nPS composite system similar to other nanoenergetic materials, which are receiving a great deal of attention for rapid energy release rates compared to bulk materials.[23−30] In addition, with a flame propagation rate up to 3050 m/s, a heat of reaction of ~11 kJ/g, and compatibility with semiconductor microfabrication techniques, nPS energetic composites are some of the most impressive nanothermite materials.[18,19,31,32]

While the initiation of the reaction and resulting heat output have been investigated by a thorough calorimetry investigation,[19] an understanding of the reactions, compositions, and temperature of the impressive flame produced during the explosion is lacking. However, recent research into the production of ball lightning (observations of buoyant fireballs accompanying lightning strikes) have used arc discharge into silicon wafers to produce fireballs in which nanoparticle silica is

formed.[33,34] Additionally, McCord et al.[17] reported generation of a white powder from an explosive reaction between nPS and concentrated HNO_3, but did not conduct analysis of this product. High-speed videos of long (7 cm) strips of nPS–$NaClO_4$ clearly reveal the presence of a fireball that persists even after the solid state reaction has traversed the length of the strip.[18] From the videos, it is evident that combustion continues in the gas phase. While a growing body of research has examined burn rates and energy output of nPS energetics, a detailed investigation of the subsequent gas phase reaction is lacking. The experiments in this paper seek specifically to examine the fireball and resulting products occurring from the solid state reaction of nPS with NaClO4 in both oxidative and inert atmospheres. The results of this study provide a more comprehensive understanding of the behavior of Si as an energetic fuel and highlight the extreme conditions that can be produced from a solid state reaction.

2. EXPERIMENTAL SECTION

2.1. nPS and nPS–$NaClO_4$ Composite Fabrication (Materials for High-Speed Video Analysis). The methods to produce the 2 mm diameter active nPS regions with integrated ignitor wire are the same as those used to fabricate long strips for burn rate tests and are discussed in a prior publication.[18] Briefly, to fabricate the selected 2 mm diameter active nPS region, 1–10 Ω·cm (100) Si wafers protected by 600 nm of low stress LPCVD Si_3N_4 were used. The Si_3N_4 served as an etch mask, and selected regions 2 mm in diameter were removed by standard microfabrication techniques to form the regions for nPS generation. Additionally, in these regions, ignitor wires made of a stack of Cr, Pt, and Au were fabricated to trigger nPS reactions.[18] The nPS is then generated with a galvanic etching technique in an electrolyte composed of 3:1 (vol:vol) of 49% HF in water to ethanol. Of the total electrolyte volume, 2.4% is composed of 30% H_2O_2 in water.

The galvanic technique relies on using the current generated by the electrochemical potential difference between the exposed Si and the platinum deposited on the backside of the wafer.[18,19,35−40] The galvanic technique is useful because Si chips of arbitrary dimensions can be etched and the etch rate is quite high, which helps minimize the time the wafer is exposed to HF that can cause damage to the metals of the ignitor wire. The chips are etched for 10 min and produce an nPS film that is ~65 µm thick as measured by SEM cross section and a porosity measured by the gravimetric method of 79−83%. Using the gas adsorption technique (Micromeritics TriStar II) with the BET method, a pore size of 2.8−2.9 nm and a surface area of 890−910 m^2/g are determined.

Following nPS formation, the chips were cleaved and then wire bonded in a standard electronics package, as seen in Figure 1a. The pores were filled with sodium perchlorate ($NaClO_4$) by immersing the entire electronics package with the bonded nPS in a 3.2 M solution of $NaClO_4$ in methanol (MeOH) for 30 s. The package is then removed from the $NaClO_4$ solution, and excess liquid is gently blown dry under a stream of N_2. To protect the packages from moisture, they are immediately placed in a commercial parylene deposition chamber (Union Carbide 10C) that is pumped down to 0.5 Torr. Approximately 5 µm of parylene is coated on the entire electronics package in a process that exposes the samples to a maximum temperature of ~50 °C.[41]

2.2. nPS and nPS–$NaClO_4$ Composite Fabrication (Materials for Reaction Product Characterization). As demonstrated in Becker et al.,[19] Si wafers of 1–10 Ω·cm resistivity with 170 nm of Pt on the backside were etched for 30 min in the same electrolyte as used for the 2 mm nPS samples. Mildly stirring the solution during etching improves uniformity of the nPS layer across the Si wafer. The Si wafers are diced in ~2 × 2 cm chips prior to etching. The nPS thickness is ~60 µm, as measured by SEM cross section, and the porosity, measured by gravimetric method, is 62−65%. Using the gas adsorption technique (Micromeritics TriStar II) with the BET method, the pore size is 2.65−2.70 nm and the surface area is ~680 m^2/g.
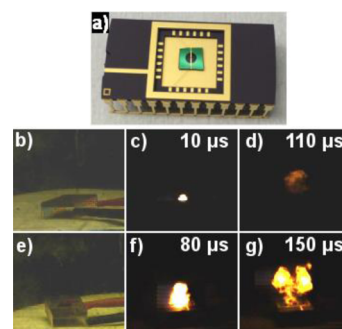
Figure 1. (a) An nPS chip with 2 mm diameter active area (the circular black region) with integrated ignitor wire. The chip is wire bonded to an electronics package so that a power supply can simultaneously trigger the reaction and start the data acquisition by a high-speed camera. The electronics package is 15 mm × 30 mm. (b–d) High-speed images of nPS–$NaClO_4$ ignition in an N_2 environment. (e–g) High-speed images of nPS–$NaClO_4$ ignition in a laboratory air environment.

The nPS was then impregnated with $NaClO_4$ by dropcasting a 3.2 M $NaClO_4$ in MeOH solution onto the nPS chip and drying for at least 15 min in an N_2-filled glovebox. Similar to the method of Becker et al.,[19] the chips of nPS–$NaClO_4$ were then placed in a stainless steel bomb (Parr Instruments, 1109A) and ignited with a nickel−chromium fuse wire (Figure S1, Supporting Information). The mass of active nPS in the bomb was estimated to range from about 10−60 mg.

2.3. nPS Combustion Characterization. For the studies requiring imaging in an N_2 environment, the nPS with $NaClO_4$ was ignited in a 30 cm × 30 cm × 45 cm plexiglass box plumbed to nitrogen (N_2) that is continuously flowed for 15 min to create a nearly oxygen (O_2)- and water (H_2O)-free environment. The images were acquired using a Photron Fastcam SA5 camera. The Schlieren imaging system is a single-mirror coincident beam setup with a 41 cm diameter spherical mirror and 113 cm focal length. Further details and schematic of the system are provided in Muramoto et al.[42] Images were acquired using a Photron Fastcam APX RS camera.

2.4. Thermodynamic Calculations. Cheetah 6.0[43] developed by Lawrence Livermore National Laboratory was used for chemical equilibrium calculations. The calculations were performed at adiabatic and constant pressure (1 atm) conditions using the JCZS library. The constant pressure condition is used to simulate the unconfined environment in which the high-speed videos of the reaction were captured.

2.5. nPS Reaction Product Characterization. The X-ray diffraction analysis was performed on a Rigaku Ultima III diffractometer (Cu Kα radiation). The TGA analysis was conducted on a PerkinElmer TGA7 at a heating rate of 5 °C/min from 25 to 1000 °C under a stream of either N_2 or clean dry air with a flow rate of 20.0 mL/min. The initial sample mass was 5.052 and 4.140 mg of nPS for the N_2 and air experiments, respectively. The Raman analysis was conducted using a Renishaw InVia system with an 1800 lines/mm grating and a 514 nm laser capable of 200 mW. The laser power was kept to the minimum while still maintaining good signal-to-noise and avoiding inducing peak shifts. The nPS reaction products are robust but have low signal intensity and are analyzed under a 50× microscope objective with 5 accumulations of 300s and 50% laser power. The nPS itself is susceptible to heat induced stress that can shift the peaks, so it is analyzed using a 100× objective, at 0.1% laser power with 5 accumulations of 300 s. The SEM image is captured on a Hitachi S-4500 microscope. The TEM work is performed on an FEI Tecnai T12 with a Bruker SDD EDX detector.

3. RESULTS AND DISCUSSION

3.1. High-Speed Video. The details of the 2 mm diameter nPS fabrication for high-speed video studies are presented in the Experimental Section and are similar to prior studies.[18] To

record the fireball above the nPS explosion, the packaged 2 mm nPS wafer chips (the active nPS region is the circular black region), as shown in Figure 1a, were ignited both in laboratory air and in a plexiglass box plumbed with N_2 gas to greatly reduce the O_2 and H_2O content in the atmosphere. The samples are ignited by supplying 21 V across the ignitor wire with a Keithley 2400 power supply. The power supply simultaneously triggers the high-speed camera to record and the nPS to ignite. Figure 1b−d and Figure 1e−f show the resulting fireball in the N_2 and air environments, respectively, recorded at 100 000 frames per second (fps). The time stamps on the images are relative to the first visible light emission from the reaction.

In the N_2 atmosphere, the fireball is nearly extinguished by 110 μs, whereas, in air, the fireball is still very luminous at 150 μs. The experiments were repeated twice. In an air environment, the fireball is visible for 1.1 and 1.4 ms, but in N_2, the fireball is visible for only 0.3 ms in both experiments. It is important to note that the duration the flame is visible in the video is related to the frame rate of the video capture. Higher frame rates reduce the amount of light the camera can capture, so the times must be compared under the same camera settings.

As Figure 1g and Video S1 (see the Supporting Information) taken in air at 100 000 fps show, the fireball splits into two distinct regions that eventually extinguish in an almost spiral fashion. The higher resolution Video S2 (see the Supporting Information), taken in air at 10 000 fps, also shows generation of a fireball that coalesces into luminous particles that persist and appear to float after the main fireball has extinguished, also in a spiral fashion.

Next, a Schlieren imaging system was used at 12 000 fps to determine if a shock wave is produced by the nPS explosion in laboratory air. The images in Figure 2 reveal that a shock wave
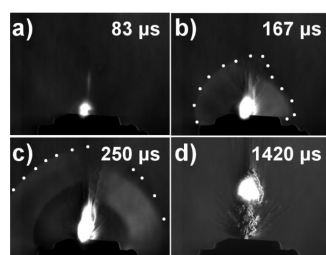

Figure 2. Selected images acquired in laboratory air at the labeled time stamps in (a−d) from Schlieren videography of combustion of a 2 mm diameter nPS−NaClO$_4$ active area (as shown in Figure 1a).

is indeed produced from the explosion. The nearly vertical sliver of light in Figure 2a is from the lighting system in the Schlieren setup and unrelated to the explosion. The superimposed white dots are to aid in visualizing the front of the shock wave and help to highlight a discontinuity in the shock wave in the vicinity of a high density of hot material ejected by the explosion. An additional test conducted at 30 000 fps was used to determine that the speed of the shock wave is 1127 ± 113 m/s, which corresponds to a Mach number of 3.3 for a speed of sound in air of 340 m/s. Using eq 1, the temperature reached in a normal shock wave at this velocity is calculated as 605 °C.[44]

$$\frac{T_1}{T_0} = \frac{[2\gamma M^2 - (\gamma - 1)][(\gamma - 1)M^2 + 2]}{(\gamma + 1)^2 M^2} \tag{1}$$

In eq 1, M is the Mach number and γ is the specific heat ratio of air under a constant pressure process divided by a constant volume process (c_p/c_v) and is equal to 1.4 for air. T_1 is the temperature downstream of the shock wave, and T_0 is the temperature upstream.

To further understand the oxidation of nPS, TGA measurements were carried out in N_2 and air atmospheres, and the resulting weight gain versus temperature results are shown in Figure 3. As seen by the steep rise in weight gain, oxidation in
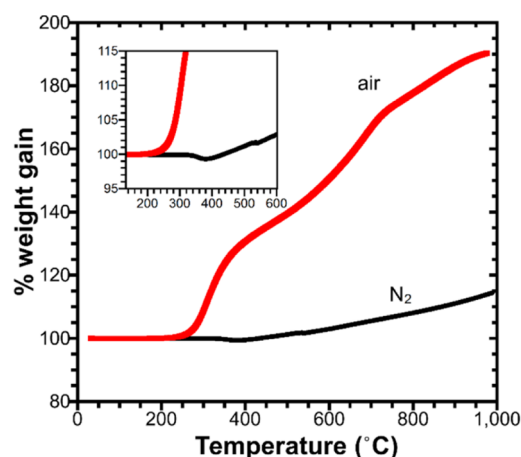

Figure 3. TGA trace of nPS in air and in N_2. The inset focuses on the lower temperature region.

air begins near 220 °C, which is well below the calculated temperature of the shock wave of 605 °C. Therefore, if there is unreacted nPS that is ejected from the substrate, it will likely combust as a result of heating from the shock wave. This oxidation may partly be responsible for the fireball observed and increased thermal output measured from reacting nPS in air or O_2.[19] In the N_2 environment, the slight weight loss observed near 340 °C is the result of H_2 desorption from the surface, as a prior study using FTIR and DSC revealed,[19] and is proceeded by a slight weight gain. The lack of a large weight gain, indicative of a limited reaction, in an N_2 atmosphere correlates well to the high-speed videos that show a much smaller and shorter duration fireball in N_2 compared to O_2.

3.2. Thermodynamic Calculations. While the high velocity and subsequent temperature rise of the shock wave may help to directly oxidize ejected unreacted nPS from the nPS−NaClO$_4$ combustion, other reactive products may be formed that further oxidize in a secondary gas phase reaction. To evaluate these products, Cheetah 6.0 was used to calculate reaction temperatures, gas volume production, and products from the reaction.

In the most basic form, the energetic reaction of nPS with NaClO$_4$ occurs according to eq 2.

$$2Si + NaClO_4 \rightarrow 2SiO_2 + NaCl \tag{2}$$
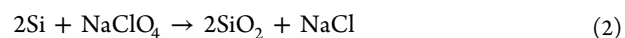
While NaClO$_4$ typically has a crystal H_2O, DSC analysis from a previous study showed that, when dried under N_2, no crystal H_2O is present in NaClO$_4$, and therefore, H_2O is not included in the Cheetah 6.0 thermodynamic calculations.[19] Figure 4a,b shows the results of the calculations for the evolved temperature and gas volume and the mole fraction of products, respectively. The trace products are primarily SiO$_2$ and Na$_2$Cl$_2$ gases. Currently, controlling the exact fuel:oxidizer ratio is difficult since incorporating NaClO$_4$ relies on wicking a MeOH
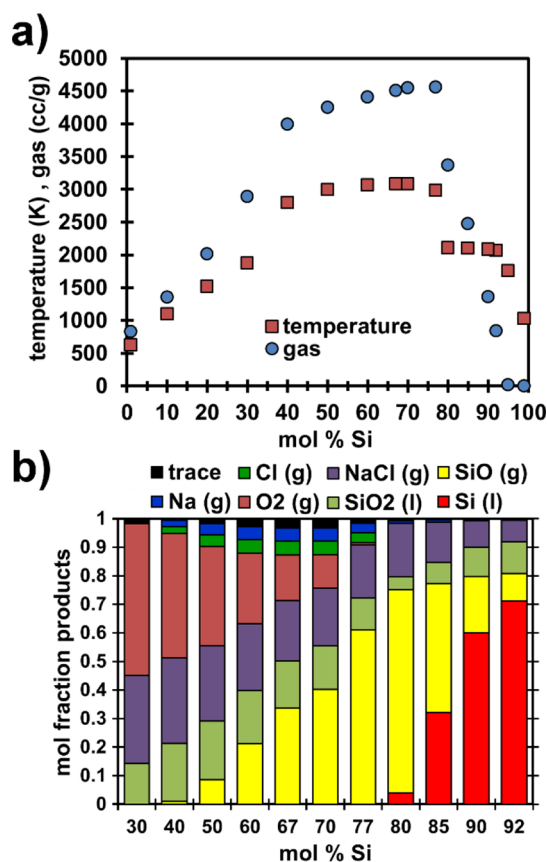
Figure 4. (a) Temperature (K) and gas (cc/g) evolved from an nPS−NaClO$_4$ reaction. (b) Mole fraction of products from an nPS−NaClO$_4$ reaction.

based solution of NaClO$_4$ into the pores and is likely to have variability. A prior study, however, did place the nPS−NaClO$_4$ ratio between 92 and 77 mol % Si.[19] These limits in addition to the theoretical equivalence ratio where the moles of fuel and oxidizer are balanced at 67 mol % Si are included in Figure 4. In the 92 mol % Si case, a 0.71 mole fraction of liquid Si is produced with the remainder being SiO and NaCl gas and liquid SiO$_2$. The temperature reaches 2060 K, and 840 cc/g of gas is produced, which is a dramatic jump from 95 mol % Si, which only produces 180 cc/g of gas and 1760 K. Liquid Si is present in the products down to 80 mol % Si, but between 80 and 77 mol %, liquid Si is no longer present as a dramatic rise in SiO is observed. Additionally, at 77 mol % Si, 4560 cc/g of gas is produced, and the temperature reaches 2980 K. Moving down the equivalence point, the temperature and gas evolution remain roughly constant at 3080 K and 4510 cc/g, and most notably in the products, O$_2$ gas is evolved, which may serve to oxidize unreacted Si.

The thermodynamic calculation results presented here are similar to those of a previous report by Mason et al., in which the additional crystal H$_2$O of NaClO$_4$ was included.[27] As a result of the H$_2$O, the authors report H$_2$ gas generation but still have a maximum temperature near 3000 K. Contrary to the results of Figure 4b, Mason et al. does not report O$_2$ gas generation, likely because it reacts with H$_2$. The authors also note that the dissociation of liquid SiO$_2$ to gaseous products limits the maximum temperature to 3000 K. It is interesting that, even with H$_2$O present, the maximum temperature is similar to that calculated in Figure 4a; in burn rate tests from

our research group, unless the samples are dried completely, either the burn rate is very slow or the nPS simply will not ignite.

Still images taken from a high-speed video (Video S2, Supporting Information) of the nPS combustion in air are shown in Figure 5a−e. This video, which is taken with different
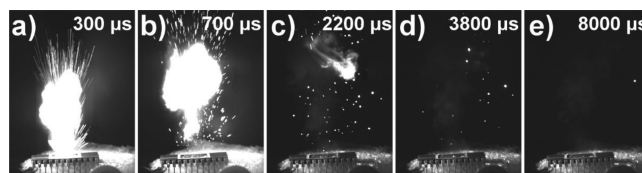

Figure 5. High-speed video captures at the labeled time stamps (a−e) of a 2 mm nPS−NaClO$_4$ ignition in air.

lighting effects than in Figure 1 and is 10 times slower at 10 000 frames per second, shows that a considerable fireball of after-burning products is produced. Figure 5c also shows that the main fireball ceases the upward trajectory and spirals until it extinguishes. The most obvious candidates for the reactants in the fireball are liquid Si and gaseous SiO, which would fully oxidize in the presence of O$_2$ at the elevated temperatures from the reaction. Additionally, unreacted solid nPS that has been mechanically shattered from the chip may contribute to the combustion as it is heated by the shock wave. Experimentally, the molar percentage of Si in the nPS−NaClO$_4$ composite has been found to lie between 77% and 92%, although this was for nPS prepared from slightly different etching conditions.[19] Regardless, according to the results from Figure 4b for this molar percentage range, SiO and liquid Si are the prime candidates for continued combustion above the initial explosion.

3.3. Reaction Products. The solid products of the explosive reaction have not been studied. For this reason, nPS−NaClO$_4$ composites are ignited inside a calorimeter bomb where the reaction products can easily be collected. The details of the nPS used for this part of the study are found in the Experimental Section. The samples were ignited in the bomb under two distinct atmospheres: (1) filled only with N$_2$ at atmospheric pressure by sealing the samples while in a standard glovebox or (2) filled with a mixture of N$_2$ from the glovebox and 40 psig (as measured by the gas cylinder regulator) of O$_2$ gas. This pressure was chosen to create an environment that can oxidize unreacted nPS in the fireball, but is low enough to avoid spontaneous ignition of the nPS−NaClO$_4$ composite.[19] In both atmospheres, the solid products inside the bomb after the reaction consist of shattered Si substrate and clumps of a white fluffy powder, although there was typically greater amounts of white powder when O$_2$ was used. The powder resulting from the reaction in the calorimeter bomb with 40 psig of O$_2$ is shown in Figure 6 with an SEM image and an optical image inset. The figure is representative of products from both N$_2$ and 40 psig O$_2$ atmospheres.

In addition to testing the nPS chips, to eliminate possible contamination of the powder product from small pieces of shattered Si substrate, nPS films were scraped from the Si substrate to create nPS powder. Approximately 10−60 mg of nPS powder was subsequently mixed with ~0.3 mL of 3.2 M NaClO$_4$ in MeOH to create a stoichiometrically balanced reaction (see the Supporting Information for calculations). The mixture is made in the steel reaction bomb and allowed to dry
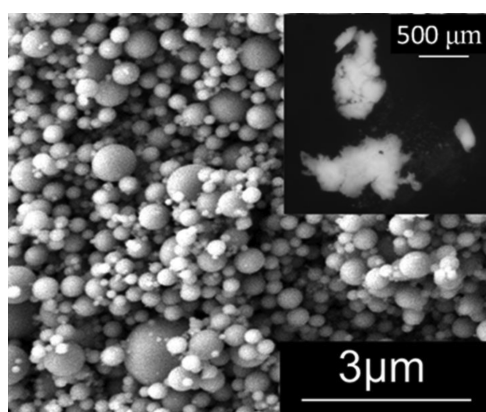
Figure 6. SEM image, with optical inset of the powder residue from the nPS−NaClO$_4$ composite reacted in the stainless steel calorimeter bomb with 40 psig of O$_2$.

for at least 15 min in the N$_2$ glovebox prior to igniting with the fuse wire. The XRD spectra taken of the nPS powder precombustion and of the combustion products are shown in Figure 7a. Prior to combustion, the XRD peaks have a broad
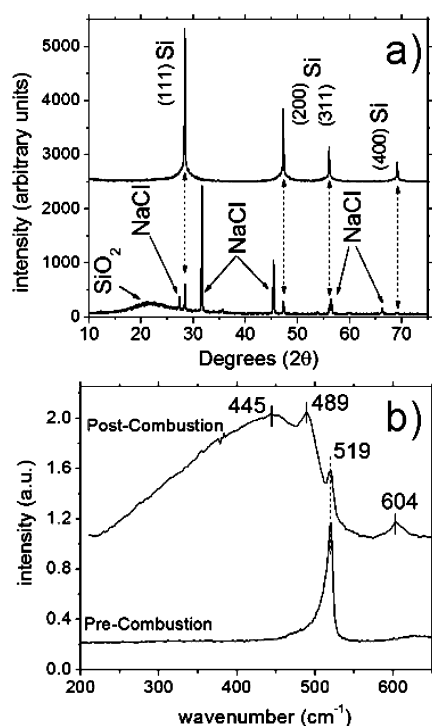
Figure 7. (a) XRD spectra of nPS (top) and of products from nPS−NaClO$_4$ after combustion (bottom) and (b) Raman spectra of nPS precombustion and nPS−NaClO$_4$ postcombustion.

base that tapers to a sharp peak, similar to spectra reported previously for nPS.[45,46] Using a Scherrer analysis, the sizes of the domains for the (111) sharp peak and broad base are 120 and 6 nm, respectively. After the ignition, only one size domain of 120 nm is present, which likely arises from traces of unreacted Si in the XRD sample.

Additionally, in the XRD spectrum, the broad hump centered near 21° 2θ indicates amorphous SiO$_2$, as previously observed by Cisneros et al. after heating nPS in O$_2$ from 300 to 700 °C.[15] Cisneros et al. also observed amorphous Si while heating from

300 to 700 °C; however, both the amorphous Si and the SiO$_2$ contributions vanished as crystalline SiO$_2$ appeared upon heating to 900 °C. Some caution should be used in comparing results as the experiments by Cisneros et al. were conducted on lower surface area nPS (∼284 m^2/g) with larger pores (5.3 nm), thus resulting in larger crystalline domains as compared to the samples here. However, amorphous Si or crystalline SiO$_2$ was not observed in the present samples by Raman spectroscopy or XRD analyses, which indicates that the nPS−NaClO$_4$ reaction is fundamentally different from the comparatively slow oxidation of nPS in an O$_2$ atmosphere studied by Cisneros et al.

Raman spectra of nPS precombustion and nPS−NaClO$_4$ postcombustion are shown in Figure 7b. The postcombustion spectrum shows a large, broad peak at 445 cm^{-1} and two smaller, sharp peaks at 489 and 604 cm^{-1}, a peak pattern characteristic of fumed silica.[47] The peak at 489 cm^{-1} is indicative of ring structures in the amorphous SiO$_2$ network, and the slight increase in intensity relative to the peak at 445 cm^{-1} is representative of nanostructured fumed silica.[48] In both spectra, a sharp peak at 519 cm^{-1} results from single crystal Si and indicates that unreacted Si remains in the product.

As a final comparison, chips of just nPS without NaClO$_4$ were placed in the bomb and then filled with 400 psig of O$_2$ to ensure complete combustion (see the Supporting Information for calculations). The oxidation reaction is then triggered by the ignition wire. The powder mixture is brown prior to combustion, and is converted to a white powder after combustion that is similar to that seen with the nPS−NaClO$_4$ composite combustion product in Figure 6. As shown by TEM images in Figure 8a,c and Figure 8b,d
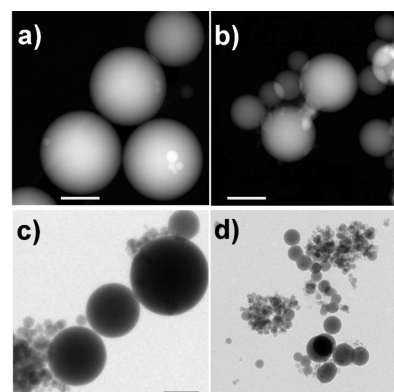
Figure 8. Reaction products of nPS combustion imaged by TEM. Images (a) and (c) are of nPS combustion products without NaClO$_4$ but in an atmosphere of 400 psig O$_2$. Images (b) and (d) are of nPS−NaClO$_4$ combustion products with 40 psig of O$_2$ or in and atmosphere of only N$_2$, respectively. All scale bars are 200 nm.

(additional images Figures S2 and S3, Supporting Information), the resulting particles do not appear significantly different whether the chips of nPS are ignited in high pressure O$_2$ without NaClO$_4$ or as a composite with NaClO$_4$, respectively. An analysis by Raman spectroscopy produced identical results to those shown in Figure 7b. One difference is that particles with necks and that appear to be joined are not seen in the products of nPS reacted with only O$_2$. The EDS of the samples (Figure S4, Supporting Information) reveals that the particles are composed of Si and O. In particles with the neck region, some Na is observed, but it remains unclear if this is a sodium silicate compound or contamination. The TEM images of

samples ignited with NaClO$_4$ show crystals of most likely NaCl (Figure S5, Supporting Information). The TEM and SEM images show a broad size distribution regardless of the atmosphere conditions during ignition. Qualitatively, when ignited with excess O$_2$, the calorimeter bomb contains much more white powder after the ignition than without excess O$_2$. This result agrees with previous research that shows that, when ignited in an O$_2$ environment, a greater energy release occurs, indicative of a more complete combustion.[19]

The fact that particles larger than several hundred nanometers are produced from a solid state material composed of single nanometer diameter pores is very interesting. The product resembles that of fumed silica. Nanometer scale silica materials, especially fumed silica, have also received a great deal of attention in both fundamental and applied research.[47,49] Fumed silica is typically produced by combusting silicon tetrachloride in an O$_2$/H$_2$ flame to yield a white, powdery solid composed of nanometer scale amorphous silica particles, often linked together, forming larger agglomerates.[47] The particles here highlight the fact that likely a gas phase reaction proceeds once the solid state reaction between NaClO$_4$ and nPS occurs. Additionally, in the case where only high pressure O$_2$ is used to ignite the nPS in a pressure vessel with an igniter wire, there must be enough heat generated to combust the nPS thin film and convert the nPS into gas or liquid phase SiO, SiO$_2$, or liquid phase Si, as predicted thermodynamically in Figure 4b. Since there appears to be additional combustion in the gas phase, as evidenced by a large flame in an air atmosphere, it is likely that at least a portion of the SiO$_x$ particles are generated from SiO gas and liquid Si rather than entirely from liquid droplets of SiO$_2$ that will simply cool rather than continue to oxidize.

4. CONCLUSION

In summary, the reaction of nPS with NaClO$_4$ and with and without excess O$_2$ has been analyzed. High-speed camera images reveal significant after burning of products ejected into an air atmosphere as opposed to an inert N$_2$ atmosphere. This indicates that there is combustion of unreacted nPS that subsequently oxidizes as it is heated from the reaction or that there are reactive species, likely liquid Si or gaseous SiO, as revealed by thermodynamic calculations. A shock wave is identified by Schlieren video work, and the velocity of the shock wave will lead to a large enough temperature rise to readily ignite unreacted nPS that is ejected from the substrate. Additionally, the solid products of the combustion reaction of nPS were studied by igniting nPS in both chip and powder forms and with and without O$_2$ environments. The white, fluffy powder product, characteristic of amorphous silica, is found to be composed of particles of a nearly perfect spherical shape with polydisperse sizes ranging from just under 50 nm to upward of 1000 nm. The resulting products all showed very similar morphologies with possible formation of sodium silicate necks that join particles. Future work might examine different morphologies of nPS or different oxidizing salts to determine if the particle size of SiO$_2$ can be controlled or unique products formed. Other interesting work might include introducing reactive species into a gas headspace to create nanoparticles of varying chemical composition.

■ ASSOCIATED CONTENT

⑤ Supporting Information

The Supporting Information is available free of charge on the ACS Publications website at DOI: 10.1021/acsami.5b09076.

> Additional TEM and EDS data and further details on the nPS reaction (PDF)
> Video of the explosive nPS−NaClO$_4$ in air taken at 1 00 000 fps (AVI)
> Video of the explosive nPS−NaClO$_4$ in air taken at 10 000 fps (AVI)

■ AUTHOR INFORMATION

Corresponding Author

*E-mail: Collin.r.becker.civ@mail.mil.

Notes

The authors declare no competing financial interest.

■ REFERENCES

(1) Canham, L., Ed. *Properties of Porous Silicon*; EMIS Datareviews Series; INSPEC: London, 1997.

(2) Canham, L. T. Silicon Quantum Wire Array Fabrication by Electrochemical and Chemical Dissolution of Wafers. *Appl. Phys. Lett.* **1990**, *57* (10), 1046.

(3) Lehmann, V.; Gosele, U. Porous Silicon Formation - a Quantum Wire Effect. *Appl. Phys. Lett.* **1991**, *58* (8), 856−858.

(4) Moghaddam, S.; Pengwang, E.; Jiang, Y.-B.; Garcia, A. R.; Burnett, D. J.; Brinker, C. J.; Masel, R. I.; Shannon, M. A. An Inorganic-Organic Proton Exchange Membrane for Fuel Cells with a Controlled Nanoscale Pore Structure. *Nat. Nanotechnol.* **2010**, *5* (3), 230−236.

(5) Orosco, M. M.; Pacholski, C.; Sailor, M. J. Real-Time Monitoring of Enzyme Activity in a Mesoporous Silicon Double Layer. *Nat. Nanotechnol.* **2009**, *4* (4), 255−258.

(6) Ge, M.; Rong, J.; Fang, X.; Zhou, C. Porous Doped Silicon Nanowires for Lithium Ion Battery Anode with Long Cycle Life. *Nano Lett.* **2012**, *12* (5), 2318−2323.

(7) Shin, H. C.; Corno, J. A.; Gole, J. L.; Liu, M. L. Porous Silicon Negative Electrodes for Rechargeable Lithium Batteries. *J. Power Sources* **2005**, *139* (1−2), 314−320.

(8) Singh, P.; Sharma, S.; Ravindra, N. M. Applications of Porous Silicon Thin Films in Solar Cells and Biosensors. *JOM* **2010**, *62* (6), 15−24.

(9) Park, J. H.; Gu, L.; von Maltzahn, G.; Ruoslahti, E.; Bhatia, S. N.; Sailor, M. J. Biodegradable Luminescent Porous Silicon Nanoparticles for in Vivo Applications. *Nat. Mater.* **2009**, *8* (4), 331−336.

(10) Sailor, M. J. Preparation of Micro-, Meso-, and Macro-Porous Silicon Layers. In *Porous Silicon in Practice*; Wiley-VCH Verlag GmbH & Co. KGaA: Weinheim, Germany, 2011; pp 43−76.

(11) Ge, M.; Rong, J.; Fang, X.; Zhang, A.; Lu, Y.; Zhou, C. Scalable Preparation of Porous Silicon Nanoparticles and Their Application for Lithium-Ion Battery Anodes. *Nano Res.* **2013**, *6* (3), 174−181.

(12) Farrell, D.; Limaye, S.; Subramanian, S. Porous Silicon Particles. U.S. Patent US20060251562A1, November 9, 2006.

(13) Salonen, J.; Lehto, V. P.; Laine, E. Thermal Oxidation of Free-Standing Porous Silicon Films. *Appl. Phys. Lett.* **1997**, *70* (5), 637−639.

(14) Arita, Y.; Kuranari, K.; Sunohara, Y. Thermal-Behavior of Porous Silicon. *Jpn. J. Appl. Phys.* **1976**, *15* (9), 1655−1664.

(15) Cisneros, R.; Pfeiffer, H.; Wang, C. M. Oxygen Absorption in Free-Standing Porous Silicon: A Structural, Optical and Kinetic Analysis. *Nanoscale Res. Lett.* **2010**, *5* (4), 686−691.

(16) Kovalev, D.; Timoshenko, V. Y.; Kunzner, N.; Gross, E.; Koch, F. Strong Explosive Interaction of Hydrogenated Porous Silicon with Oxygen at Cryogenic Temperatures. *Phys. Rev. Lett.* **2001**, *87* (6), 068301.

(17) McCord, P.; Yau, S.-L.; Bard, A. J. Chemiluminescence of Anodized and Etched Silicon: Evidence for a Luminescent Siloxene-Like Layer on Porous Silicon. *Science* **1992**, *257* (5066), 68−69.

(18) Becker, C. R.; Apperson, S.; Morris, C. J.; Gangopadhyay, S.; Currano, L. J.; Churaman, W. A.; Stoldt, C. R. Galvanic Porous Silicon Composites for High-Velocity Nanoenergetics. *Nano Lett.* **2011**, *11* (2), 803−807.

(19) Becker, C. R.; Currano, L. J.; Churaman, W. A.; Stoldt, C. R. Thermal Analysis of the Exothermic Reaction between Galvanic Porous Silicon and Sodium Perchlorate. *ACS Appl. Mater. Interfaces* **2010**, *2* (11), 2998−3003.

(20) Mikulec, F. V.; Kirtland, J. D.; Sailor, M. J. Explosive Nanocrystalline Porous Silicon and Its Use in Atomic Emission Spectroscopy. *Adv. Mater.* **2002**, *14* (1), 38−41.

(21) Clement, D.; Diener, J.; Gross, E.; Kunzner, N.; Timoshenko, V. Y.; Kovalev, D. Highly Explosive Nanosilicon-Based Composite Materials. *Phys. Status Solidi A* **2005**, *202* (8), 1357−1364.

(22) Plummer, A.; Kuznetsov, V.; Joyner, T.; Shapter, J.; Voelcker, N. H. The Burning Rate of Energetic Films of Nanostructured Porous Silicon. *Small* **2011**, *7* (23), 3392−3398.

(23) Apperson, S.; Shende, R. V.; Subramanian, S.; Tappmeyer, D.; Gangopadhyay, S.; Chen, Z.; Gangopadhyay, K.; Redner, P.; Nicholich, S.; Kapoor, D. Generation of Fast Propagating Combustion and Shock Waves with Copper Oxide/aluminum Nanothermite Composites. *Appl. Phys. Lett.* **2007**, *91* (24), 243109.

(24) Son, S. F.; Asay, B. W.; Foley, T. J.; Yetter, R. A.; Wu, M. H.; Risha, G. A. Combustion of Nanoscale Al/MoO3 Thermite in Microchannels. *J. Propul. Power* **2007**, *23* (4), 715−721.

(25) Sullivan, K.; Zachariah, M. R. Simultaneous Pressure and Optical Measurements of Nanoaluminum Thermites: Investigating the Reaction Mechanism. *J. Propul. Power* **2010**, *26* (3), 467−472.

(26) Rossi, C.; Zhang, K.; Esteve, D.; Alphonse, P.; Tailhades, P.; Vahlas, C. Nanoenergetic Materials for MEMS: A Review. *J. Microelectromech. Syst.* **2007**, *16*, 919−931.

(27) Mason, B. A.; Groven, L. J.; Son, S. F.; Yetter, R. A. Combustion Performance of Several Nanosilicon-Based Nanoenergetics. *J. Propul. Power* **2013**, *29* (6), 1435−1444.

(28) Marín, L.; Nanayakkara, C. E.; Veyan, J.-F.; Warot-Fonrose, B.; Joulie, S.; Estève, A.; Tenailleau, C.; Chabal, Y. J.; Rossi, C. Enhancing the Reactivity of Al/CuO Nanolaminates by Cu Incorporation at the Interfaces. *ACS Appl. Mater. Interfaces* **2015**, *7* (22), 11713−11718.

(29) Patel, V. K.; Bhattacharya, S. High-Performance Nanothermite Composites Based on Aloe-Vera-Directed CuO Nanorods. *ACS Appl. Mater. Interfaces* **2013**, *5* (24), 13364−13374.

(30) Wang, L.; Luss, D.; Martirosyan, K. S. The Behavior of Nanothermite Reaction Based on Bi2O3/Al. *J. Appl. Phys.* **2011**, *110* (7), 074311.

(31) Piekiel, N. W.; Morris, C. J. Small-Scale, Self-Propagating Combustion Realized with On-Chip Porous Silicon. *ACS Appl. Mater. Interfaces* **2015**, *7* (18), 9889−9897.

(32) Piekiel, N. W.; Morris, C. J.; Currano, L. J.; Lunking, D. M.; Isaacson, B.; Churaman, W. A. Enhancement of on-Chip Combustion via Nanoporous Silicon Microchannels. *Combust. Flame* **2014**, *161* (5), 1417−1424.

(33) Abrahamson, J.; Dinniss, J. Ball Lightning Caused by Oxidation of Nanoparticle Networks from Normal Lightning Strikes on Soil. *Nature* **2000**, *403* (6769), 519−521.

(34) Ito, T.; Cappelli, M. A. Nanoparticle Production in Arc Generated Fireballs of Granular Silicon Powder. *AIP Adv.* **2012**, *2* (1), 012126.

(35) Becker, C. R.; Miller, D. C.; Stoldt, C. R. Galvanically Coupled Gold/silicon-on-Insulator Microstructures in Hydrofluoric Acid Electrolytes: Finite Element Simulation and Morphological Analysis of Electrochemical Corrosion. *J. Micromech. Microeng.* **2010**, *20* (8), 085017.

(36) Miller, D. C.; Becker, C. R.; Stoldt, C. R. Relation Between Morphology, Etch Rate, Surface Wetting, and Electrochemical Characteristics for Micromachined Silicon Subject to Galvanic Corrosion. *J. Electrochem. Soc.* **2008**, *155* (12), F253−F265.

(37) Ashruf, C. M. A.; French, P. J.; Bressers, P.; Kelly, J. J. Galvanic Porous Silicon Formation without External Contacts. *Sens. Actuators, A* **1999**, *74* (1−3), 118−122.

(38) Splinter, A.; Sturmann, J.; Benecke, W. New Porous Silicon Formation Technology Using Internal Current Generation with Galvanic Elements. *Sens. Actuators, A* **2001**, *92* (1−3), 394−399.

(39) Kelly, J. J.; Xia, X. H.; Ashruf, C. M. A.; French, P. J. Galvanic Cell Formation: A Review of Approaches to Silicon Etching for Sensor Fabrication. *IEEE Sens. J.* **2001**, *1* (2), 127−142.

(40) Kolasinski, K. Porous Silicon Formation by Galvanic Etching. In *Handbook of Porous Silicon*; Canham, L., Ed.; Springer International Publishing: Cham, Switzerland, 2014; pp 23−33.

(41) Churaman, W.; Becker, C. R.; Morris, C. J.; Currano, L. J.; Wu, C.-C.; Sailor, M. J. Packaging Nanoporous Energetic Silicon For On-Chip Mems Applications. In *International Wafer-Level Packaging Conference 2011 Proceedings*, Santa Clara, CA, Oct 3−6, 2011; SMTA: Edina, MN, 2011.

(42) Muramoto, S.; Forbes, T. P.; Staymates, M. E.; Gillen, G. Visualizing Mass Transport in Desorption Electrospray Ionization Using Time-of-Flight Secondary Ion Mass Spectrometry. *Analyst* **2014**, *139* (11), 2668.

(43) Bastea, S.; Fried, L. E.; Glaesemann, K. R.; Howard, W. M.; Kuo, I-F.W.; Souers, P. C.; Vitello, P. A. *Cheetah 6.0 User's Manual*; Lawrence Livermore National Laboratory, U.S. Department of Energy: Livermore, CA, 2010.

(44) *Equations, Tables and Charts for Compressible Flow*; Report NACA 1135; Ames Aeronautical Laboratory: Moffett Field, CA, 1953.

(45) Ogata, Y. H.; Yoshimi, N.; Yasuda, R.; Tsuboi, T.; Sakka, T.; Otsuki, A. Structural Change in P-Type Porous Silicon by Thermal Annealing. *J. Appl. Phys.* **2001**, *90* (12), 6487−6492.

(46) Lehmann, V.; Jobst, B.; Muschik, T.; Kux, A.; Petrova-Koch, V. Correlation between Optical Properties and Crystallite Size in Porous Silicon. *Jpn. J. Appl. Phys.* **1993**, *32* (5A), 2095−2099.

(47) Vaccaro, G.; Agnello, S.; Buscarino, G.; Gelardi, F. M. Thermally Induced Structural Modification of Silica Nanoparticles Investigated by Raman and Infrared Absorption Spectroscopies. *J. Phys. Chem. C* **2010**, *114* (33), 13991−13997.

(48) Buscarino, G.; Ardizzone, V.; Vaccaro, G.; Agnello, S.; Gelardi, F. M. Atomic Force Microscopy and Raman Investigation on the Sintering Process of Amorphous SiO2 Nanoparticles. *J. Appl. Phys.* **2010**, *108* (7), 074314.

(49) Seipenbusch, M.; Rothenbacher, S.; Kirchhoff, M.; Schmid, H. J.; Kasper, G.; Weber, A. P. Interparticle Forces in Silica Nanoparticle Agglomerates. *J. Nanopart. Res.* **2010**, *12* (6), 2037−2044.